View metadata, citation and similar papers at core.ac.uk
brought to you by CORE
provided by University of Queensland eSpace

5th Australasian Congress on Applied Mechanics, ACAM 2007
10-12 December 2007, Brisbane, Australia

Applications of Mechanics and Modelling to Biomechanical Themes

Mark J Pearcy

School of Engineering Systems and Institute of Health and Biomedical Innovation,
Queensland University of Technology, Brisbane, Australia

Abstract: This paper examines the application of mechanics to model the behaviour of the human body. Understanding of this behaviour is necessary in order to improve medical interventions for injury and disease that affect the daily function of an individual. Modelling techniques are presented that enable predictions of how the tissues of the body respond to changes in their mechanical environment. Finite element methods are often used to model both hard and soft tissues and it is important to understand the limitations of these techniques but also their power in predicting responses that may lead to improvements in health care. Examples are presented of modelling plates to fix broken bones, how the next generation of artificial limbs might be attached directly to the skeleton and how osteoporosis affects the strength of the spine.

Keywords: biomechanics, modelling, fracture healing, spinal mechanics, osteoporosis, artificial limbs, osseointegration

1 Introduction

Measurement of the mechanics of the human body is difficult due to the complicated structure of the body and the complex properties of the tissues it is made from. Medical interventions for mechanical disorders often involve the implantation of engineered materials to provide temporary mechanical support, such as metal plates to support a fractured bone, or permanent replacement, such as an artificial hip joint. These devices must interface with the biology of the body in a way that is neither detrimental to the host nor to the device. This ‘biocompatibility’ has a chemical component and a mechanical component. The materials can be designed to be relatively inert biochemically but the response of the tissues to a changed mechanical environment needs careful consideration. This paper examines a number of examples where the application of mechanics through modelling studies is shedding light on how to deal with difficult medical conditions.

Modelling of the combination of bones and fracture fixation devices can lead to an understanding of how the mechanical environment the bone experiences affects the healing response and this is a major area of study around the world. Combinations of finite element modelling with algorithms to model the biological response to the mechanical stresses and strains are being developed to understand how best to assist a fracture to heal.

Leading on from the innovations in dental implants where titanium pins are inserted into the jaw to provide an anchor for artificial teeth, this technology is now being applied to the attachment of artificial limbs. An implant can be inserted into the residual limb and an artificial limb attached to the implant. It is important that the forces transmitted through the implant to the bone are kept below a level that would damage the bone. Physical measurements of the forces experienced by the limb combined with modelling of the implant-bone interface are able to provide insights into the design of the implant.

The body also undergoes changes due to age and disease that affect its mechanics. Osteoporosis can compromise the strength of the bone in the spine to the extent that the vertebral bodies collapse under the loads experienced in normal activities. To develop effective treatments it is necessary to understand how the structure of the bone is altered by osteoporosis and how the changes in structure relate to the changed mechanics.

This paper looks at a number of these examples to provide an insight into how mechanical concepts are being applied to improve the quality of life for patients with mechanical disorders.

2 Application of mechanics to biomechanical conditions

Three examples of the application of mechanics and modelling are presented to show the potential for biomechanical analysis to improve clinical treatment.

2.1 Numerical Investigation of Osteoporosis under Plate Fixation Devices in a Sheep Tibia by a Remodeling Theory

Gongfa Chen[1], Beat Schmutz[1], Mark J Pearcy[1] ,Michael A Schütz[1,2]
[1]School of Engineering Systems and Institute of Health and Biomedical Innovation, Queensland University of Technology, Brisbane, Australia
[2]Department of Orthopaedics, Princess Alexandra Hospital, Brisbane, Australia

2.1.1 Introduction

Metal plates screwed onto a bone across a fracture are a standard technique for treating some fractures of long bones. Osteoporosis under this plate fixation is a well known occurrence that causes weakening of bone [1-6]. Hence, if a plate is left on too long the bone may refracture due to this weakening [7]. Two hypotheses have been proposed to explain it: stress-shielding induced by the plate [8] and an inadequate blood supply caused by plating [9-11]. This study aimed to establish a numerical algorithm based on a bone remodeling theory to investigate osteoporosis under a plate used for the internal fixation of fractures. A numerical algorithm is proposed to predict the bone remodeling process [12] under the stress-shielding condition induced by plating. The remodeling process is simulated by numerous discrete steps of the bone adaptation to the actual mechanical stimulus. At each step, a finite element analysis is conducted to determine the stress tensor and strain tensor. The patterns of the mechanical stimulus and the bone density change are obtained, and the relation between stress-shielding and osteoporosis is investigated. The influences of plate stiffness on osteoporosis development are studied.

2.1.2 Method

In the remodeling process, it is assumed that bone adapts to the actual mechanical stimulus. This process can be described with a generic mathematical expression, using the apparent density as the characterization of the internal morphology. It is assumed that this stimulus is directly related to the local mechanical load in the bone and can be determined from the local stress tensor and strain tensor. The rate of change of the apparent density of the bone at a particular location, dρ/dt, can be specified by [18]:

$$\frac{d\rho}{dt} = B\left(\frac{S}{\rho} - k\right) \qquad 0 < \rho < \rho_{\max} \quad (1)$$

where B is a constant which characterises the remodeling rate and ρ_{max} is the maximum density of a bone. Here $S = S(x,y,z)$ is the strain energy density (SED) and k, the reference SED. The Young's modulus (E) of a bone is related to its density (ρ) by:

$$E = C.\rho^r \qquad (2)$$

where C is a constant and $r = 2$ is used in this paper [13].

A sheep tibia model with a plate was created. An intact bone was used in this study to remove the complexity of the fracture so that the osteoporotic changes in the bone could be seen clearly. A 3-dimensional intact bone model was constructed from the CT-images of the left hind tibia of a 6-year-old Merino-Cross ewe, with a weight of 27.8 kg (CT scanned at 120KVP and a spacing of 0.5 mm for the axial slices. The pixel size was 0.4 x 0.4 mm). A solid model of the cortical bone was generated from the CT-image data using the software packages Amira (Mercury Computer Systems Inc.) and Geomagic Studio (Raindrop Geomagic Inc.). The method of constructing the solid model was described in Messmer et al [14]. As the main concerns are the stress distribution around the plate, the proximal and distal ends of the bone were not included.

A LCP 3.5 plate (Synthes), 7 holes, was used. It has a length of 98 mm, width of 11 mm, and thickness of 3 mm. In the simulations, the plate was slightly simplified. The hole shape was re-

constructed with 2 semi-circles (4.4 mm in diameter) and 2 straight lines. Some rounds/fillets along the plate's edges were removed. The modifications were not expected to change the plate stiffness significantly.

In the simulations, the screw was represented by a two-level cylinder with a head part and a body part. It was assumed that the head part and the body part were firmly connected to the plate and the bone respectively. The diameter of the body part was 2.9 mm, which is the core diameter of a LCP locking screw (Ø 3.5 mm). The diameter of the head part was the same as that of the plate holes. The total length of the screws was 10 mm, with the body part being 7 mm.

The solid models of the bone, plate and screws were assembled in SolidWorks (SolidWorks Corporation). The plate was positioned medially as close as possible to the bone. At each end of the plate, two uni-cortical screws were inserted at the corresponding positions of the locking screws in the actual plate. The assembly was imported into ABAQUS as a Parasolid. The contact between the plate/bone interface was simulated by contact elements; the coefficient of friction was 0.4 [9].

A stainless steel plate was modelled for this study with a Young's modulus of 200 GPa. The Poisson ratio was 0.3. The screws were also steel with a Young's modulus of 200 GPa and Poisson ratio 0.3. The Young's modulus of the cortex was determined by the remodeling process.

The proximal end was completely constrained. A 273 N (body weight) axial compressive force was applied to the distal end of the model. It was assumed to be the maximum load applied to the sheep tibia during the gait cycle, and was applied as a constant static load throughout the analysis. As the tibia is bowed slightly from the posterior side to the anterior side; a uniformly distributed force would cause bending in the middle of the tibia. It is believed that long bones are loaded in axial compression and it is muscle that counteracts the external bending moment [15-17]. As no muscle forces were considered in this paper, it was more logical to assume that the compressive force was non-uniformly distributed along the anteroposterior axis on the distal end, which minimizes the bending moment in the tibia. The maximum and minimum normal stresses on the distal end were 3.5 MPa and 0.5 MPa respectively.

It was assumed that the maximum bone density of the cortex, ρ_{max} = 1.8 gcm^{-3} and the corresponding Young's modulus was 20 GPa [18]. Hence the constant C in Equation (2) was 6173 MPa $(gcm^{-3})^{-2}$. The initial bone density was taken to be 1.7 gcm^{-3}, which gave an initial Young's modulus of 18 GPa. The Poisson ratio was taken to be 0.3 for the entire remodeling process. The bone was assumed isotropic. The simulation was divided into three steps. The first step was of a short time period (0.01day), in which the external load was set up and kept unchanged in the following process; a static analysis was conducted for the intact bone without plating. The strain energy density, S, was calculated and the value of S/ρ stored at each Gauss integration point. It was assumed that the intact bone was in remodeling equilibrium under the initial loading condition. Hence, the saved S/ρ was used as the reference value, k, in the following process. Consequently, k is site-specific.

The second step was also of a short time period (0.01 day), in which the plate was added to the model, the stress was re-distributed and the stress unloading patterns obtained. As this step was very short, the remodelling was not included.

The remodeling process was simulated in the third step, which simulated 360 days. This step was divided into 180 increments. In each iteration, the stress analysis was conducted and the value of S/ρ was calculated. By using Equation (1), the remodeling rate and the density change were obtained for the bone; the Young's modulus was updated according to Equation (2) for the next iteration. The detailed implementation of the remodelling process in ABAQUS was described in Chen et al [19]. The constant, B, which characterizes the remodeling rate, was calibrated with previous experimental results. The mass density of a bone plated with a titanium plate reduces to around 90 % in 12 months [3-5]. Therefore, B was adjusted to give an overall 10 % bone loss in 360 days. In this paper, B was 2.5 $(gcm^{-3})^2$/(MPa day).

2.1.3 Results

The development of osteoporosis for the bone plated with the steel plate is illustrated in Figure 1. At 360 days, the bone loss in the region under the plate was 9 % and around the screw holes, the greatest loss was 11 %. At 360 days, the bone growth on the side opposite to plating was about 2 %.

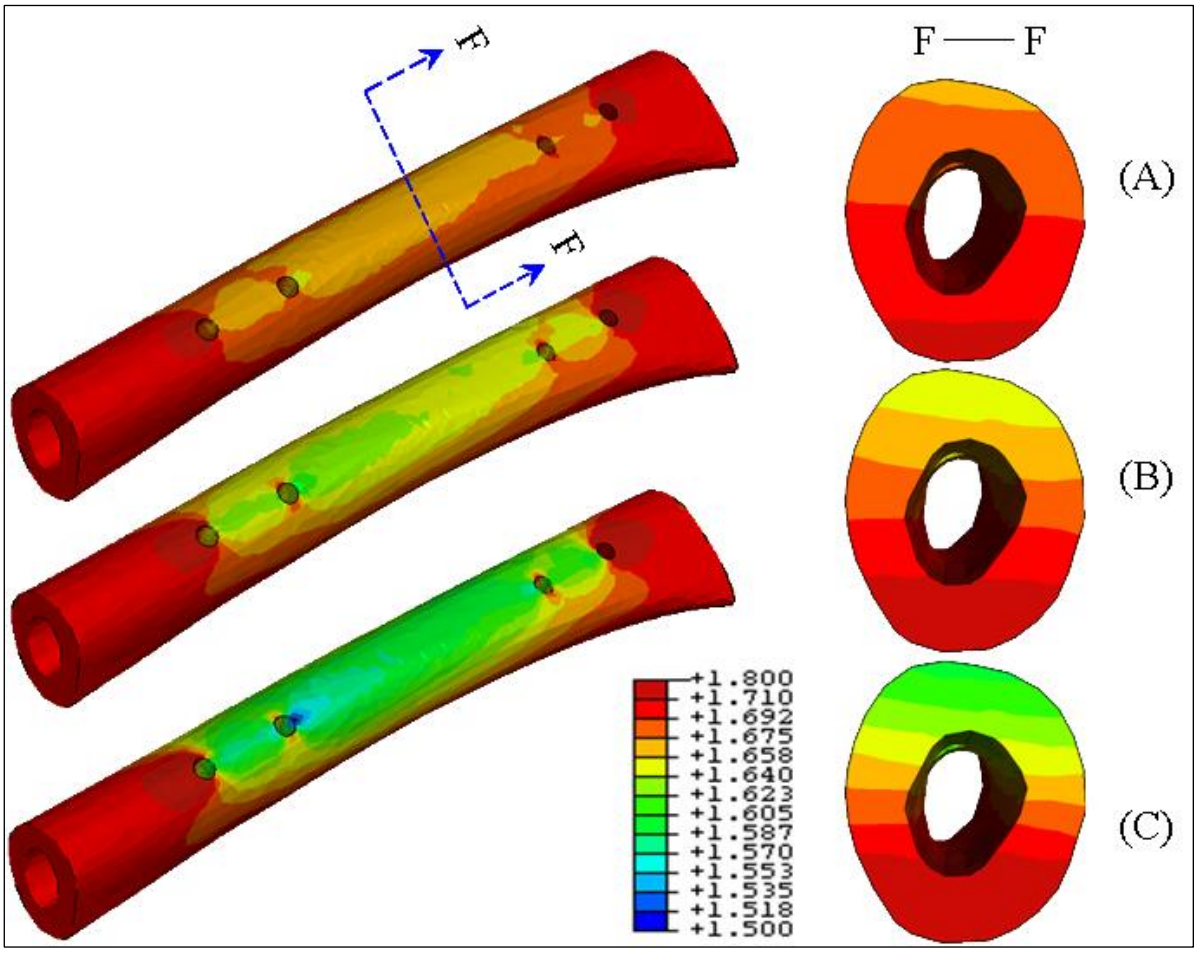

Figure 1. Porosis development after plating with a steel plate. The right column shows the contour plot of bone density on the cross section F-F. (A) At 100 days; (B) At 200 days; (C) At 360 days.

2.1.4 Discussion

The results demonstrate that, for a stiff plate, the stress reduction was significant between the two outermost screws as was expected and this led to significant loss of density. Owing to stress concentration on the outer half surface of the outermost screw holes, bone growth has been observed in this region and increases in density were seen in the simulation.

Beside stress-shielding with plating, other mechanisms may exist for osteoporosis. Applying a plate onto a long bone would impair the periosteal blood supply to the bone [20]. Perren [9] assumed that the impaired periosteal blood supply induces cortical porosis. The contact between the plate and the bone is a possible mechanism of impedance of blood supply to bone cortex. The two processes probably affect the bone concurrently.

The plate-screw-bone interfaces were assumed to be ideal; real load transfer mechanisms through the interfaces will be more complex than this. Though the remodeling theories have certain limitations, they still provide useful explanations for how the plating induces the osteoporosis. This study suggests that osteoporosis can be explained as a result of a load-dependent biological process.

2.2 FE Stress Analysis of the Interface Between the Bone and an Osseointegrated Implant for Amputees

Winson CC Lee[1] , Jacinta M Doocey[1], Laurent A Frossard[1], Rickard Brånemark[2] , Clayton J Adam[1] , John H Evans[1] , Mark J Pearcy[1]

[1]School of Engineering Systems and Institute of Health and Biomedical innovation, Queensland University of Technology, Brisbane, Australia

[2]Centre of Orthopaedic Osseointegration, Sahlgrenska University Hospital, Goteborg, Sweden

2.2.1 Introduction

A lower-limb prosthesis is conventionally attached to the residual limb by a prosthetic socket and often with accessory suspension devices. Although this approach has been used for more than a century, residual limb pain and soft tissue breakdown due to imperfect prosthetic socket fitting are common [21-23]. In addition, fitting problems have been found to occur due to insufficient length or fluctuations in volume of the residual limb. In an attempt to solve these problems, methods to connect the prosthesis to the femur have been developed [24,25]. These methods rely on firm attachment of the implant through on-growth of the bone on to the implant known as *osseointegration*. One method currently available uses a titanium threaded implant, and a coupling device (abutment) which protrudes through the soft tissues and skin to connect with the external prosthetic components [25].

In addition to alleviating the skin problems and residual limb pain because of the absence of the prosthetic socket, studies have also shown that amputees using transfemoral osseointegrated prostheses can enjoy a greater range of hip motion and better sitting comfort compared to patients with the socket-type prosthesis [26,27]. Amputees also experience improved sensory feedback through osseoperception, can walk further and be more active than amputees using a conventional prosthesis [25, 27,28].

The direct anchorage of a lower-limb prosthesis to the bone has been shown to be an excellent alternative for amputees experiencing complications in using a conventional prosthetic socket. After surgical implantation, amputees have to undergo an initial weight bearing exercise program (that takes approximately 3 months) to promote bone-remodelling and prepare the bone to tolerate the forces likely to be developed during walking. Currently, the load magnitude acting on the abutment prescribed by the clinician for this period is measured by a domestic weight scale which measures only the vertical force. However, this does not fully replicate the patterns of loads exerted on the abutment during walking.

Osseointegrated fixation includes a coupling device (abutment) which protrudes through the soft tissues and skin to enable connection with the external prosthetic components. Unlike the internal implant for hip replacement with the entire metallic component embedded within the body, this protrusion gives a unique opportunity to perform direct load measurement on the abutment. Load applied on the abutment when the amputees perform weight bearing exercises and various activities were measured. This current study made use of the load data to study the bone-implant interface stress using computational FE models, with a motivation to suggest refinements to the rehabilitation process in order to shorten it, and to provide information for the design of the implant to avoid potential damage to the bone/implant interface.

2.2.2 Methods

Loads exerted on the abutment during weight bearing exercises and normal walking of two unilateral transfemoral amputees using osseointegrated prostheses were measured. Detailed procedures of the load measurement are described elsewhere [29-31]. In weight bearing exercises, the two subjects were asked to transfer body mass against a weigh scale through the abutment at magnitudes approaching their full body weight. The three-dimensional forces and moments were measured simultaneously using a six channel commercial force transducer (Model 45E15A; JR3 Inc., Woodland, CA). The load data were averaged for five loading trials. The three-dimensional loads applied on the abutment during straight-line, level, walking were measured by the same commercial transducer, which was mounted between the abutment and the prosthetic knee. The loads were averaged over 10 walking steps on the prosthetic limb during steady-state walking.

Using the measured load data, quasi-static implicit Finite Element (FE) analysis was performed in ABAQUS v6.6 FE package (ABAQUS Inc, RI, USA) to investigate the bone-implant interface stresses. Details of the model are as follows (Figure 2):

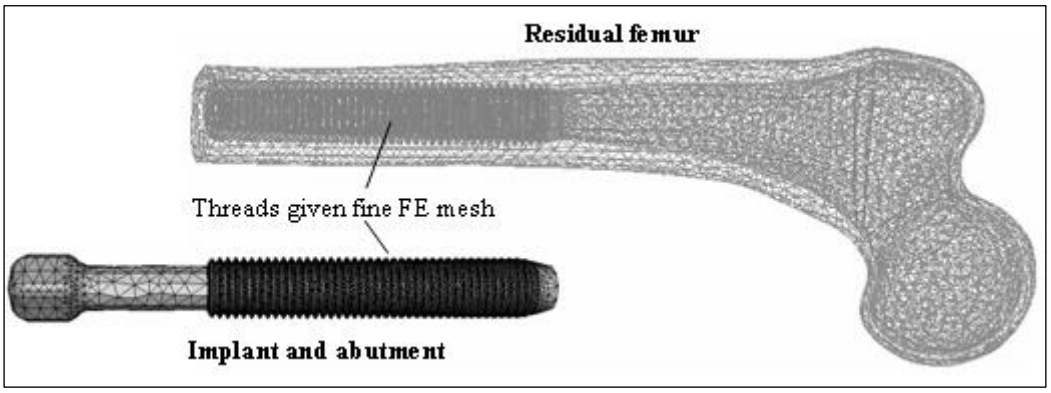

Figure 2 – Views of the meshed femur and implant.

Geometry

The geometry of the implant-abutment fixation was created in Solidworks (Solidworks Corporation, MA, USA). A generic model of the implant was created with a length of 100mm, diameter of 20mm and thread pitch of 1.75mm. To simplify the model, parallel circumferential grooves were used instead of helical threads on both the implant and the bone. The implant and the abutment were assumed to be one piece because this study focused on the bone-implant interface. A generic bone geometry was downloaded from the BEL Repository. It was a third-generation standardized femur size #3306 with an intramedullary canal. The residual bone had a length of 230mm measuring from the greater trochanter to the distal cut end. Threads on the femur were generated by geometrically subtracting the bone from the threaded implant. The threaded implant and the intramedullary canal of the femur were tied together to prevent any relative motion between the nodes at the interface.

Mesh

A FE mesh with three-dimensional tetrahedral elements was built using ABAQUS auto-meshing techniques. The optimal mesh density at the bone-implant interface was determined by performing a mesh refinement test such that convergence of peak stress was within 2% of the previous coarser mesh. A coarser mesh density was assigned to the rest of the model.

Material properties

The femur and implant were assumed to be linearly elastic and homogeneous. The femur was assumed to be transversely isotropic with a longitudinal elastic modulus of 17GPa, and a shear modulus of 11.5GPa [32,33]. The radial and circumferential moduli were assumed to be 3.28GPa. The implant was assumed to be isotropic assigned with a Young's modus of 115GPa, resembling the mechanical property of pure titanium [34,35]. A Poisson's ratio of 0.3 was used for the two structures.

Loadings and boundary conditions

Loading, based on the experimental measurements for the two subjects, was applied at the distal end of the abutment. The maximum forces encountered in weight bearing exercises were compared with a series of quasi-static loads encountered during straight-line, level walking. For walking twenty load data points were used as inputs, with more data points distributed around the local maxima of the varying forces and moments. The femoral head was fully fixed.

2.2.3 Results

The FE model calculated the stress magnitude and distribution at the bone-implant interface for the different loading cases. Peak von Mises stresses were found at the proximal end of the implanted region for both participants in all cases. Stress ratio, von Mises stress (kPa) divided by body weight (kg), is used to describe the stress magnitude.

Simulated axial-only force during weight bearing rehabilitation produced evenly distributed stresses on the bone adjacent to the implant. When the true three-dimensional forces and moments from the weight bearing exercises were examined it was found that the stress distribution on the implanted region of the bone in both subjects was less uniform. Generally higher stresses were found at the lateral aspect of the bone. The peak stress for both subjects was four times higher than for axial-only load.

During walking stresses peaked at the late stance phase of the gait (approximately 50% of the gait cycle), reaching 89.7kPa/kg for subject 1 and 92.0kPa/kg for subject 2. Figure 3 shows the typical stress distribution at late stance phase of the gait for subject 2. The stresses at the posterolateral and anteromedial regions of the interface were significantly lower than the stresses along the posteromedial and anterolateral regions. Across the gait cycle similar patterns of stress were seen, although the location of the higher nodal stress regions varied considerably.

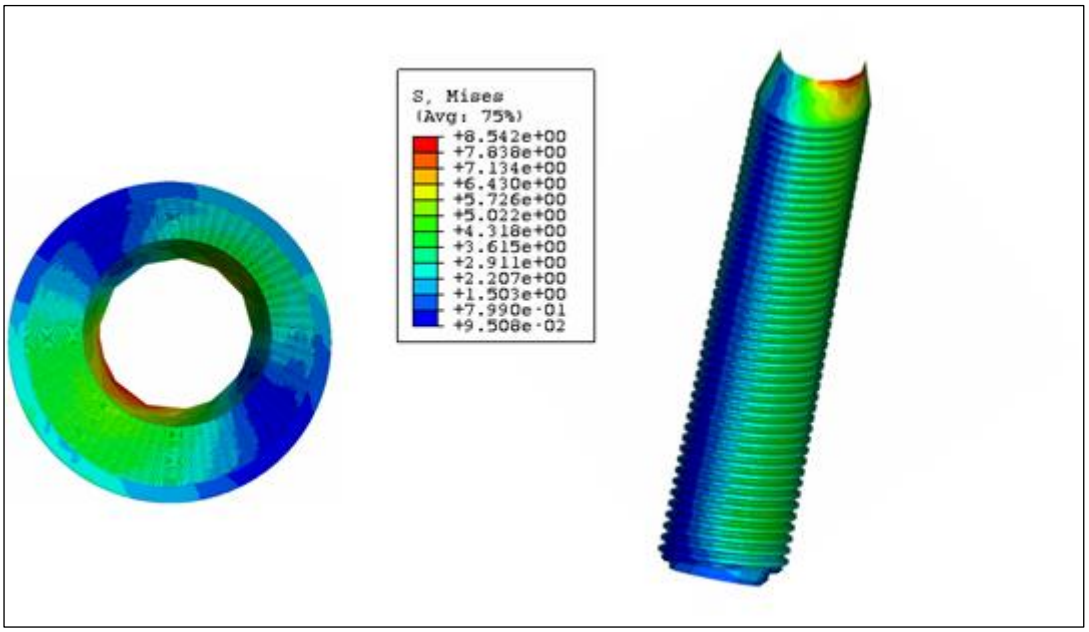

Figure 3 – Bottom view (left)and section view (right) of the stress distribution on the implanted region of the bone for subject 2 during late stance phase of the gait. (Units in legend are MPa)

2.2.4 Discussion and Conclusion

The rehabilitation program prescribes axial only force initially. However, in practice this appears hard to achieve and the resulting three-dimensional loads produce an uneven stress distribution along the implant and higher stresses than for an axial only load. This indicates that the rehabilitation program controlled by visual feedback from a weigh scale may in fact be applying significantly higher stresses than intended and so this study has provided information for the redesign of the rehabilitation program.

During walking, while the peak magnitudes of the stresses were similar to the peak stresses in the rehabilitation exercises the regions of higher stress fell at different aspects of the implanted region at different times in the gait cycle. During the rehabilitation program high stresses applied to the bone should be avoided as they can produce pain and potential loosening of the implant. However, these results suggest that suitable stress levels should be applied to appropriate regions of the bone so as to prepare for walking without the perception of pain and the potential for failure.

A generic femur geometry was used in this study. For future studies patient specific advice on a suitable rehabilitation program would be possible through the use of 3-D CT reconstruction of that individual's residual femur. The CT analysis would provide detailed geometry and material properties for the femur, and further research using CT is planned to assess if such data is of value for clinical modelling on an individual patient basis.

2.3 The Effect of Trabecular Micro-Architecture on Vertebra Biomechanics: A Finite Element Investigation

Katrina McDonald, Mark J Pearcy, Clayton J Adam
Schoool of Engineering Systems and Institute of Health and Biomedical Innovation, Queensland University of Technology, Brisbane, Australia

2.3.1 Introduction

Osteoporosis is a disease which compromises bone mineral density and trabecular micro-architecture, resulting in increased fragility and susceptibility to fracture. 700,000 vertebral fractures occur each year in the United States alone, 85% of which are associated with osteoporosis. Osteoporosis results in thinning of the trabeculae, increased spacing between trabeculae, and thinning of the cortical shell of the vertebrae. Although the microarchitectural changes have been thoroughly explored, the effects of these changes on whole vertebra biomechanics are still not well understood.

This study presents the development of a microstructural model of an entire lumbar vertebral body to investigate the effects of osteoporotic changes in bone micro-architecture on vertebral biomechanics, specifically, the change in stiffness, stresses and load sharing capacity of the core and cortex.

Previous studies have either modelled small sections of trabecular bone or developed macro-structural models of whole vertebrae. For the first time, this study employs a combination of beam elements to represent the trabecular micro-architecture, and shell elements to represent the vertebral cortex, to create a realistic, micro-structural vertebra model. The paper presents the development of this microstructural model of an entire lumbar vertebral body and preliminary simulations to investigate the effects of changes in trabecular bone micro-architecture on the vertebral stiffness, stresses around the cortex, and load carriage between the vertebral cortex and trabecular core.

2.3.2 Methods

A finite element model of an L3 human lumbar vertebral body was created using equations given by Mizrahi [36] for the vertebral body geometry. In Mizrahi's study, a parametric approach was used to create an idealised cortex geometry that was a general population representation, and that did not have the computational difficulty associated with models derived from images. Four sets of equations were used to describe the nonuniform taper of the cortical shell, the endplate curvature and the "tear-drop" cross section geometry. This created a parametric vertebral body which did not include the posterior elements, as they have been shown to play a minor role in axial compression loading [37]. To ensure the cortex was an accurate representation of an L3 vertebral body, the geometry was compared with published values of human vertebral geometry in the literature [38-40]. The greatest geometric dimensional difference between the parametric model and a human vertebra was 15%, with an average variation of 7%. This was considered a reasonable approximation. The model was shelled to a thickness of 0.68mm to represent the thickness of the cortical wall [41]. The vertebral cortex was meshed using 2.5mm triangular shell elements.

The internal trabecular microstructure was created by generating a three dimensional matrix of nodes. The spacing between nodes in each plane was determined using values published by Mosekilde [42]. Different spacing values were used for the transverse and longitudinal planes. Three models were produced with age representative trabecular spacings and diameters to characterise trabecular microarchitecture at age <50, age 50 to 75, and age >75 years. An additional perturbation was added to the coordinates of each node in the trabecular microstructure, to provide a degree of random irregularity in the structure, as occurs in real bone. The perturbation value defines how far each node is able to move along each plane from its original coordinate. Hence a low perturbation results in a relatively square matrix whilst a high perturbation gives an irregular matrix. Jenson [43] found perturbation values between 0.4 and 0.8 to be most appropriate for human trabecular bone, and therefore a perturbation value of 0.6 was employed for the model. This allowed each node point to move by ±30% of the original spacing value in each plane.

Three dimensional beam elements were added between the node points to create a three dimensional lattice. The beam thickness values were set to correspond with the models of various ages. These values were again acquired from published values by Mosekilde [42].

The whole-vertebra models were created by incorporating the beam models into the shell cortex. Additionally, trabecular-only models were created in which the vertebral body geometry was preserved but the cortical shell was omitted, to explore load sharing between the trabecular core and shell. A shell-only model was also created which did not include a trabecular core shows the whole vertebra model, and the three trabecular structures.

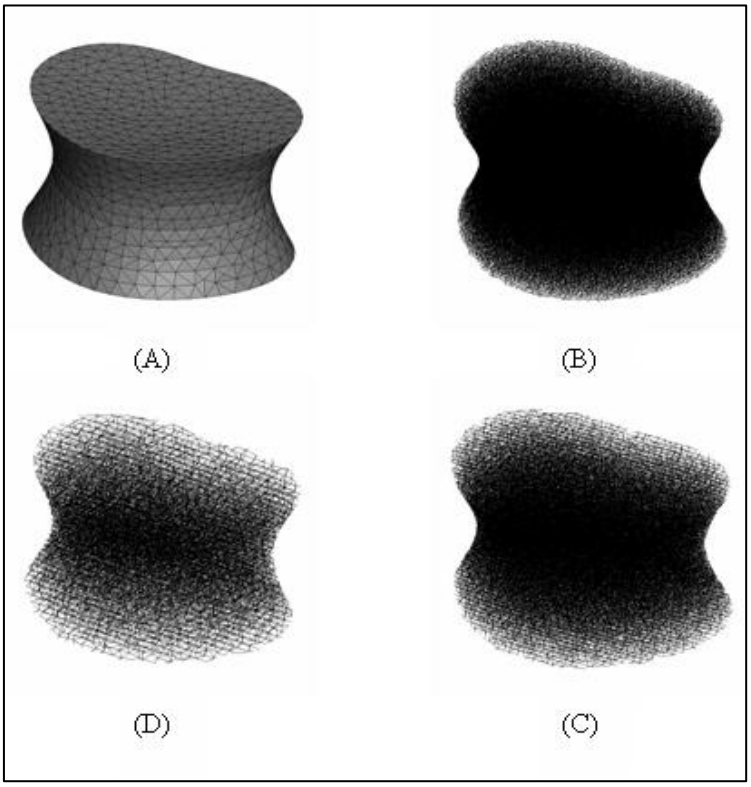

Figure 4: Finite element models created using shell and beam elements. (A. FE mesh for cortical shell. B. to D. Trabecular micro-beam models for age <50, age 50-75 and age >75 respectively)

The tissue-level material properties for both the trabecular core and cortical shell were assumed to be the same. A Young's modulus of 13GPa [44] and a Poisson's ratio of 0.3 was applied for parent bone material. The models were solved using ABAQUS/Standard (version 6.6, Abaqus Inc, RI, USA). The ABAQUS nonlinear geometry capability was used to include the effects of large deformations and displacements in solving the model.

Two loading cases were applied to each model. The first loading case was an applied displacement to the entire top endplate compressing the vertebra vertically by 1mm. This loading case simulates in-vitro compression testing, in which both endplates are rigidly potted in bone cement and an applied displacement is used to load the vertebra. The second was a uniform distribution of pressure (1MPa) over the top end plate of the vertebrae. This approximates to twice the normal load the vertebra experiences in relaxed standing for a 60kg individual, however, the 1MPa pressure allows convenient interpretation of results. In both load cases, the bottom endplate was constrained in all three degrees of freedom.

2.3.3 Results

The solutions from the displacement load cases were used to determine the total vertical reaction force at the lower endplate of the vertebra. From this, the stiffness was calculated for the trabecular-only, shell-only and vertebra models. The predicted shell-only stiffness was 26,550 N/mm. The trabecular-only stiffness and overall vertebral stiffness for the various age groups are shown in Table

1. The percentage of load carried by the trabecular core and cortical shell were also calculated for each case and is shown in Table 1.

Table 1: Stiffness values for trabecular and whole vertebra models and the percent of load carried with an applied displacement at 1mm.

Model	Trabecular-only stiffness (N/mm)	Overall vertebra stiffness (N/mm)	Load carried by trabecular core (%)	Load carried by cortex (%)
Age < 50	22,820	55,750	52	48
Age 50-75	2,690	31,460	16	84
Age > 75	690	28,200	6	94

The pressure loading simulations allowed an investigation of stresses experienced throughout the vertebra. The location and magnitude of both maximum von Mises stress and Maximum Principal stress for each model are given in Table 3.

Table 2: Maximum Von Mises stress and Maximum Principal Stress in each model with uniform applied pressure of 1MPa on the upper endplate

Model	Max.Von Mises stress (MPa)	Location	Max.Principal stress (MPa)	Location
Age < 50	9.06	Posterior-lateral region of sidewall	5.4	Posterior region of endplate and shell
Age 50-75	30.4	Posterior junction of endplate and sidewall	28.7	Intermediate ring between centre and edge of endplate .
Age > 75	79.4	Posterior junction of endplate and sidewall	73.2	Intermediate ring between centre and edge of endplate
Shell-only	175.7	Posterior junction of endplate and sidewall	153.4	Intermediate ring between centre and edge of endplate

2.3.4 Discussion

The FE results showed that age-related reductions in trabecular thickness and increases in trabecular spacing dramatically reduce the stiffness of the trabecular core, and vertebral body as a whole. Further, the proportion of total load carried by the trabecular core diminished from 52% in the age<50 model to a negligible amount for the age>75 model. The model results to date compare favourably with existing literature [45, 46].

The results presented in this paper are preliminary findings obtained during the early developmental stages of this model, and the limitations should be recognised. The cortical shell is an idealised geometry based on a mathematical description in the literature and not based on any real vertebral anatomy. While the initial results have been promising, and have been in general agreement with the literature, further development and validation of the model is required. To achieve this, CT and micro-CT imaging will be used to scan human lumbar vertebrae, measure the overall anatomy and internal micro-architecture, and determine the spatial distribution of trabecular thickness and spacing through the vertebral body. Mechanical testing will then be performed on the human vertebra and the model predictions will be validated against FE results for the same specimen. Once validated, the modelling techniques presented in this paper will be used to thoroughly investigate the effects of microarchitectural variations occurring in osteoporosis on vertebral mechanics, as well as the mechanics of current surgical techniques employed in the treatment of vertebral compression fractures.

3 Conclusion

These three case studies applying computational mechanics to clinical problems show that they offer great potential for the understanding of how the body responds to mechanical stimuli. The increase in our understanding of how the components of the body function mechanically and how they interact with one another and with implanted devices is already leading to improved designs of techniques and devices. However, care must be taken to understand the assumptions implicit in the development of a model and the importance of validation in order to produce results and recommendations that are realistic.

References

[1] Tonino AJ, Davidson CL, Klopper PJ, Linclau LA. Protection from stress in bone and its effects. Experiments with stainless steel and plastic plates in dogs. The Journal Of Bone And Joint Surgery British Volume 1976;58-B(1):107-113.

[2] Moyen BJ, Lahey PJ, Weinberg EH, Harris WH. Effects on intact femora of dogs of the application and removal of metal plates. A metabolic and structural study comparing stiffer and more flexible plates. The Journal Of Bone And Joint Surgery American Volume 1978;60(7):940-947.

[3] Uhthoff HK, Bardos DI, Liskova-Kiar M. The advantages of titanium alloy over stainless steel plates for the internal fixation of fractures. An experimental study in dogs. The Journal Of Bone And Joint Surgery British Volume 1981;63-B(3):427-484.

[4] Uhthoff HK, Finnegan M. The effects of metal plates on post-traumatic remodeling and bone mass. The Journal Of Bone And Joint Surgery British Volume 1983;65(1):66-71.

[5] Terjesen TMD, Nordby AMD, Arnulf VMD. The Extent of Stress-protection After Plate Osteosynthesis in the Human Tibia. Clinical Orthopaedics & Related Research 1986;207:108-112.

[6] Uhthoff HK, Foux A, Yeadon A, McAuley J, Black RC. Two processes of bone remodeling in plated intact femora. An experimental study in dogs. Journal of Orthopaedic Research 1993;11(1):78-91.

[7] Frankel VH, Burstein AH. The Biomechanics of Refracture of Bone. Clinical Orthopaedics & Related Research 1968;60 221-226.

[8] Uhthoff HK, Boisvert D, Finnegan M. Cortical porosis under plates. Reaction to unloading or to necrosis? The Journal Of Bone And Joint Surgery American Volume 1994;76(10):1507-1512.

[9] Perren SM, Cordey J, Rahn BA, Gautier E, Schneider E. Early temporary porosis of bone induced by internal fixation implants. A reaction to necrosis, not to stress protection? Clinical Orthopaedics And Related Research 1988(232):139-151.

[10] Gautier E, Rahn BA, Perren SM. Vascular remodeling. Injury 1995;26(Supplement 2):B11-B19.

[11] Klaue K, Fengels I, Perren SM. Long-term effects of plate osteosynthesis: comparison of four different plates. Injury 2000;31(Supplement 2):51-62.

[12] Huiskes R, Weinans H, Grootenboer HJ, Dalstra M, Fudala B, Slooff TJ. Adaptive bone-remodeling theory applied to prosthetic-design analysis. Journal of Biomechanics 1987;20(11-12):1135-1150.

[13] Rice JC, Cowin SC, Bowman JA. On the dependence of the elasticity and strength of cancellous bone on apparent density. Journal of Biomechanics 1988;21(2):155-168.

[14] Messmer P, Matthews F, Jacob AL, Kikinis R, Regazzoni P, Noser H. A CT Database for Research, Development and Education: Concept and Potential. Journal of Digital Imaging 2007;20(1):17-22.

[15] Pauwels F. Biomechanics of the locomotor apparatus: contributions on the functional anatomy of the locomotor apparatus. Berlin New York: Springer-Verlag, 1980.

[16] Taylor ME, Tanner KE, Freeman MAR, Yettram AL. Stress and strain distribution within the intact femur: compression or bending? Medical Engineering & Physics 1996;18(2):122-131.

[17] Currey JD. Bones: structure and mechanics. 2nd ed. Woodstock: Princeton University Press, 2002.

[18] Weinans H, Huiskes R, Grootenboer HJ. The behavior of adaptive bone-remodeling simulation models. Journal of Biomechanics 1992;25(12):1425-1441.

[19] Chen G, Pettet G, Pearcy M, McElwain DLS. Comparison of two numerical approaches for bone remodeling. Medical Engineering & Physics 2007;29(1):134-139.

[20] Gunst MA. Interference with bone blood supply through plating of intact bone. In: Uhthoff HK, Stahl E, editors. Current concepts of internal fixation of fractures. Berlin, New York: Springer-Verlag, 1980. p. 268-276.

[21] Gallagher, P., Allen, D. and MacLachlan, M.I., 2001. Phantom limb pain and residual limb pain following lower limb amputation: a descriptive analysis. Disability and Rehabilitation 26, 522-530.

[22] Hagberg, K. and Brånemark, R., 2001. Consequences of non-vascular trans-femoral amputation: A survey of quality of life, prosthetic use and problems. Prosthetics and Orthotics International 25, 186-194.

[23] Mak, A., Zhang, M. and Boone, D., 2001. State-of-the-art research in lower-limb prosthetic biomechanics-socket interface : A review. Journal of Rehabilitation Research & Development 38(2), 161-74.

[24] Aschoff, H. and Grundei, H., 2004. The Endo- Exo-Femurprosthesis: A new concept of prosthetic rehabilitation engineering following thigh-amputation - Some cases and early results. Int Soc for Prosthet and Orthot 11th World Congress. Hong Kong.

[25] Brånemark, R., Brånemark, P.-I., Rydevik, B.L. and Myers, R.R., 2001. Osseointegration in skeletal reconstruction and rehabilitation: A review. Journal of Rehabilitation Research and Development 38(2), 175-181.
[26] Hagberg, K., Häggström, E., Uden, M. and Brånemark, R., 2005. Socket versus bone-anchored trans-femoral prostheses: Hip range of motion and sitting comfort. Prosthetics and Orthotics International 29(2), 153-163.
[27] Sullivan, J., Uden, M., Robinson, K.P. and Sooriakumaran, S., 2003. Rehabilitation of the trans-femoral amputee with an osseointegrated prosthesis: the United Kingdom experience. Prosthetics and Orthotics International 27, 114-120.
[28] Robinson, K.P., Brånemark, R. and Ward, D.A., 2004. Future Developments: Osseointegration in Transfemoral Amputees. In: D.G. Smith, J.W. Michael and J.H. Bowker (Editors), Atlas of Amputations and Limb Deficiencies: Surgical, Prosthetic and Rehabilitation Principles. American Academy of Orthopaedic Surgeons, pp. 673-681.
[29] Cairns, N., Frossard, L., Hagberg, K. and Brånemark, R., 2006. Static load bearing during early rehabilitation of transfemoral amputees using osseointegrated fixation. In: M. Dillon (Editor), Proceedings of the 30th Annual Scientific Meeting of ISPO Australia. Keynote Conferences, The Esplanade Hotel Convention Centre, Fremantle, Western Australia.
[30] Frossard, L., Lee Gow, D., Contoyannis, B., Nunn, A. and Brånemark, R., 2003. Load applied on the abutment of transfemoral amputees fitted with an osseointegrated implant during load bearing exercises using a long pylon, International Society for Prosthetics and Orthotics-Australia, National Centre for Prosthetics and Orthotics, La Trobe University, Melbourne.
[31] Lee WCC, Frossard L, Hagberg K, Haggstrom E, Brånemark R. Kinetics Analysis of Transfemoral Amputees fitted with Osseointegrated Fixation Performing Common Activities of Daily Living. Clinical Biomechanics. 2007. In press
[32] Reilly, D.T. and Burstein, A.H., 1975. The elastic and ultimate properties of compact bone tissue. Journal of Biomechanics 8(6), 393-405.
[33] Zhang, M., Dong, X. and Fan, Y., 2005. Stress Analysis of Osseointegrated Transfemoral Prosthesis: A Finite Element Model, Proceedings of the 2005 IEEE Engineering in Medicine and Biology 27th Annual Conference, Shanghai, China.
[34] Xu, W., Crocombe, A.D. and Hughes, S.C., 2000. Finite Element Analysis of Bone Stress and Strain Around a Distal Osseointegrated Implant for Prosthetic Limb Attachment, Proceedings of the Institution of Mechanical Engineers Part H: Journal of Engineering in Medicine, pp. 595-602.
[35] Xu, W., Xu, D.H. and Crocombe, A.D., 2006. Three-dimensional finite element stress and strain analysis of a transfemoral osseointegration implant. J Eng Med 220, 661-670.
[36] Mizrahi, J., Silva, M.J., Keaveny, T.M., Edwards, W.T., Hayes, W.C., Finite-element stress analysis of the normal and osteoporotic lumbar vertebral body. Spine, **18(14)**, pp. 2088-2096. 1993.
[37] Hongo, M., Abe, E., Shimada, Y., Murai, H., Ishikawa, N., Sato, K., Surface strain distribution on thoracic and lumbar vertebrae under axial compression. The role in burst fractures. Spine, **24(12)**, pp. 1197-1202. 1999.
[38] Panjabi, M., Goel, V., Oxland, T., Takata, K., Duranceau, J., Krag, M., Price, M., Human lumbar vertebrae. Quantitative three-dimensional anatomy. Spine, **17(3)**, pp. 299-306. 1992.
[39] Zhou, S., McCarthy, I., McGregor, A., Coombs, R., Hughes, S., Geometrical dimensions of the lower lumbar vertebrae--analysis of data from digitised CT images. European Spine Journal: Official Publication Of The European Spine Society, The European Spinal Deformity Society, And The European Section Of The Cervical Spine Research Society, **9(3)**, pp. 242-248. 2000.
[40] Hall, L.T.E., Stephen I.; Noble, Philip C.; Kamaric, Emir, Morphology of the lumbar vertebral endplates. Spine, **23(14)**, pp. 1517-1522. 1998.
[41] Edwards, W.T.Z., Y; Ferrara, L A; Yuan, H A, Structural features and thickness of the vertebral cortex in the thoracolumbar spine. Spine, **26(2)**, pp. 218-225. 2001.
[42] Mosekilde, L., Sex differences in age-related loss of vertebral trabecular bone mass and structure--biomechanical consequences. Bone, **10(6)**, pp. 425-432. 1989.
[43] Jensen, K.S., Mosekilde, L., Mosekilde, L., A model of vertebral trabecular bone architecture and its mechanical properties. Bone, **11(6)**, pp. 417-423. 1990.
[44] Rho, J.Y., T.Y. Tsui, and G.M. Pharr, Elastic properties of human cortical and trabecular lamellar bone measured by nanoindentation. Biomaterials, **18(20)**, pp. 1325-1330. 1997.
[45] Rockoff, S.D., E. Sweet, and J. Bleustein, The relative contribution of trabecular and cortical bone to the strength of human lumbar vertebrae. Calcified Tissue Research, **3(2)**, pp. 163-175. 1969.
[46] Yoganandan, N., et al., Functional biomechanics of the vertebral cortex. Clinical Biomechnics, **3**, pp. 11-18. 1988.